Optical Materials 84 (2018) 636–645

Contents lists available at ScienceDirect

Optical Materials

journal homepage: www.elsevier.com/locate/optmat

Nanoparticles for Luminescent Solar Concentrators - A review

P. Moraitis[a], R.E.I. Schropp[b], W.G.J.H.M. van Sark[a,*]

[a] Copernicus Institute of Sustainable Development, Utrecht University, Utrecht, The Netherlands
[b] Debye Institute for Nanomaterials Science, Utrecht University, Utrecht, The Netherlands

ARTICLE INFO

Keywords:
Luminescent solar concentrator
Quantum dots
Solar energy
Photovoltaics

ABSTRACT

The leader of todays solar energy revolution is undoubtedly the silicon photovoltaic (PV) module. However, despite the immense progress in efficiency and the phenomenal drop of manufacturing and installation costs the dark blue flat panels have not found widespread use in the modern urban environment. The scarcity of available rooftop space, the high cost of land and the irregular metropolitan skyline have not allowed conventional solar technologies to supply cities with clean energy. Thus, new concepts are being investigated to integrate solar generators into new and existing buildings in the form of facades or windows. Luminescent Solar Concentrators (LSCs) offer a novel approach for the utilization of solar irradiation in the form of transparent glazing systems that have the potential to become functional elements of the building envelope. This paper highlights and compares the most recent technological advances in the field of LSC technology and the contribution of colloidal chemistry with reabsorption-free emitters offering broadband absorption and enhanced stability. Combined with a critical study of the newly emerged LSC applications in various fields this study will also attempt to give a possible glimpse of the near future of transparent solar harvesting devices.

1. Introduction

Solar photovoltaic (PV) technology [1] is increasingly being deployed globally leading to approximately 400 GW installed capacity at the end of 2017 [2] and this is expected to continue toward multi TW levels within a few decades [3]. PV has been reported to be a net contributor to greenhouse gas emission reduction [4], while module efficiency is gradually increasing, getting closer and closer to the Shockley-Queisser limit [5], and levelized cost of electricity is plummeting to 2–4 cents/kWh in some regions. The overall cost reduction is due to technological advances in solar cell efficiencies. Combined with lower manufacturing and installation costs have made it feasible to recover the economic investment of a roof-top PV installation on a family house in Western Europe in less than a decade [6].

However, the situation is radically different in highly urbanized or metropolitan areas, where the continuously growing demand for living space and energy to cover the needs of a constantly increasing population creates a complex operational environment for the deployment of conventional solar PV systems. Besides the high cost of land in those areas that prohibits the realization of large scale projects, it is the morphology of the urban environment itself that poses a hindering factor for solar technology in general. Modern architecture develops predominantly in terms of height creating a huge mismatch between the total volume and floor space of a building and the available rooftop area. Present-day commercial silicon modules require approximately 7 m^2 to deliver 1 kW of peak power [7], a figure that undoubtedly can have a strong impact on the energy balance of a small building but is desperately low compared to the total energy demand of modern high-rise buildings. Additionally, the irregular skyline of a metropolitan area creates complex shading patterns that further narrow the solar potential of the already limited available space.

The transition to a sustainable building sector, where energy consumption is counterbalanced by renewable energy generated on site, needs innovative solutions that are efficient, economically viable and without affecting the aesthetic appearance of the building or the quality of life of the users. The development of Building Integrated Photovoltaics (BIPV) has the potential to revolutionize urban architecture by making solar PV a structural element within the building envelope and thus transforming the outer shell into an energy production plant. BIPV as a rapidly developing sector has demonstrated a variety of different approaches and solutions, which mainly depend on crystalline silicon and thin film (in)organic PV technology [8]. But as BIPV will become an essential part of the urban landscape, the key elements for public acceptance and ultimately, financial success, will be versatility and the ability to integrate almost invisibly into new and existing buildings.

* Corresponding author.
E-mail address: w.g.j.h.m.vansark@uu.nl (W.G.J.H.M. van Sark).

https://doi.org/10.1016/j.optmat.2018.07.034
Received 15 March 2018; Received in revised form 11 July 2018; Accepted 13 July 2018

Luminescent Solar Concentrators (LSCs) enable the creation of semitransparent glazing elements that potentially transform the so far energy passive windows and facades of metropolitan buildings into electricity power generators [9,10]. The concept of LSCs was first put forward in the early 1970s as an attempt to reduce the amount of silicon required for PV modules and to drive down the overall cost of solar energy that was prohibitively high at that time [11,12]. At present, the motivation to develop LSCs is to employ their unique optical properties to camouflage solar energy devices in the urban environment, bypassing the tight operational limitations and aesthetical inflexibility of opaque and semitransparent PV modules [13].

Several excellent reviews on LSC development have been presented in the past, such as "Luminescent Solar Concentrators- A review of recent results" by Van Sark et al., in 2008 [10], "Thirty Years of Luminescent Solar Concentrator Research: Solar Energy for the Built Environment" by Debije et al. later in 2012 [14], and "Luminescent solar concentrators for building-integrated photovoltaics" in 2017 by Meinardi et al. [7]. The purpose of this paper is to review the change in the state-of-the-art of LSCs, focusing on the use of nanoparticles in LSCs, but also the recent applications that have emerged the last few years. We will first briefly describe operational principles, the past and the future of various luminophores and will close with recommendations and a future outlook.

2. Operational principle, characterization and loss mechanisms

2.1. Operational principle

A typical LSC, in its simplest form, consists of a polymer or a glass sheet acting as a waveguide with luminophores either dispersed within the sheet or coated on top [15,16]. Direct or diffuse sunlight penetrating the top surface of the matrix is absorbed by the luminophores and then is isotropically re-emitted at a longer wavelength. The emitted luminescence is guided towards the perimeter of the sheet through total internal reflection where eventually it is converted into electricity by PV cells attached along the sides, see Fig. 1. As the total LSC area that is exposed to sunlight is larger than the surface area of the cells installed on the sides, the LSC device achieves light concentration. This form of light concentration is passive and low-cost, without bulky tracking equipment. Furthermore, the inherent ability to illuminate the attached PV cells indirectly, gives to the LSC device the additional benefit of being less sensitive in shading than conventional solar cells.

2.2. Device performance

Every LSC device is characterized by the geometrical concentration factor which is defined as the $C_G = A_{LSC}/A_{PV}$, where A_{LSC} and A_{PV} are the top surface area of the matrix and the total area of solar cells, respectively. However, like any other energy conversion device, the LSC is characterized by the overall power conversion efficiency η_{device}, which is defined as the electric power P_{out}, delivered by the solar cell(s) divided by the total power of the incoming irradiation reaching the sheet P_{in}.

$$\eta_{device} = \frac{P_{out}}{P_{in}} \tag{1}$$

Commonly this quantity would be adequate to compare different LSC devices among each other or even LSCs with other concentrating technologies and conventional PV systems. However, due to the strong dependence of the incoming and delivered power on the specific geometry of each LSC, the device efficiency could be a misleading indicator if used exclusively. For a more objective comparison the electrical concentration factor C^* is used, which is the ratio between the electric power delivered by the LSC and the electric power output of the bare solar cell if it were not attached to any concentration devices under the same illumination condition of 1 Sun (AM1.5G spectrum).

$$C^* = \frac{P_{LSC}}{P_{SC}} \tag{2}$$

For the characterization of the LSC merit independently of the solar cell attached, the optical efficiency and the optical concentration factor are used. The optical efficiency η_{opt} is the ratio between the radiative power on the edge L_{Edge} of the LSC to the radiative power incident on the top surface L_{in}.

$$\eta_{opt} = \frac{L_{Edge}}{L_{in}} \tag{3}$$

It is the indicator that describes better the fundamental property of an LSC, to collect and concentrate light. However, since not every LSC shares the same physical dimensions, the concentration factor C is introduced as the product of the optical efficiency with the geometrical concentration factor C_G,

$$C = \eta_{opt} C_G \tag{4}$$

The concentration factor C can be perceived as the coefficient of effective enlargement of the area of a solar cell when it is coupled to the LSC [18], and in the case where C is larger than 1 the increased photon flux incident on the perimeter of the waveguide can boost the generated photocurrent [12,14].

The highest power conversion efficiency (PCE) that was ever reported thus far is 7.1% [19] in 2008, using a configuration with four parallel-connected GaAs solar cells, coupled to the edges of a polymethylmethacrylate (PMMA) LSC sheet doped with a mixture of two organic dye luminophores and dimensions 50 mm × 50 mm × 5 mm. A comparable PCE (6.7%) was achieved using four gallium indium phosphide (GaInP) solar cells in a multi-dye stacked configuration of two smaller plates of 20 mm × 20 mm × 3 mm [20]. A number of experimental devices have also been presented with PCE values ranging from 4.2% to 6.8% with either single or stacked LSC configuration but without any of them exceeding 14 cm × 14 cm in total surface area [20–23]. In a few cases, relatively larger devices 40 cm × 40 cm have exhibited efficiency values up to 4% with the use of back reflectors [15]. However, due to a number of losses, efficiency values remain significantly lower than the corresponding conventional solar PV and the reported dimensions of the concentrators are still far below those of a practical, commercial window.

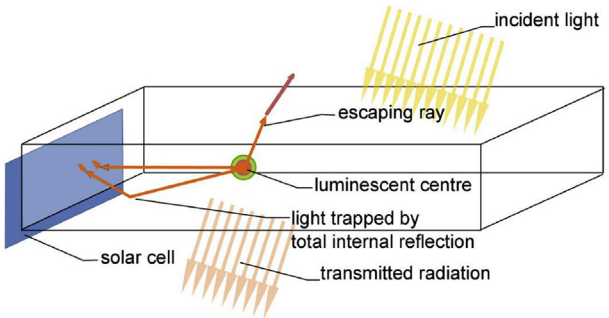

Fig. 1. Schematic representation of an LSC device under illumination [17].

2.3. Losses

Several loss mechanisms can be identified that are responsible for the final device efficiency. First, before light enters the waveguide a part of the incoming irradiation that is equal with $[(n-1)/(n+1)]^2$ will be reflected from the top surface, where n is the refractive index [24], following the Fresnel equations. However, considering that the LSC matrix is commonly made either of glass or plastic, with a refractive index close to 1.5, Fresnel losses will not exceed 3.9%. The amount of light that will be absorbed by the luminophores inside the

LSC matrix is given by the Lambert-Beer law and is proportional to the thickness of the sheet and the molar absorption coefficient ε of the luminophores at the given wavelength [25],

$$A = 1 - 10^{-\varepsilon c x} \tag{5}$$

where x is the optical path length of light through the LSC and c the concentration of the luminophores. Light that is not absorbed by the luminophores will simply travel through the waveguide as if it was a regular transparent piece of glass. The light absorption could be increased by increasing the thickness of the sheet but that would dramatically decrease the concentration factor C of the device. Nevertheless, not every absorbed photon will be re-emitted as some of the generated excitons will recombine non-radiatively. The ratio of the absorbed photons $N_{absorbed}$ and the number of emitted photons $N_{emitted}$ gives the luminescence quantum efficiency (LQE) of the luminophore.

The fundamental trapping mechanism of an LSC is based on total internal reflection, which occurs according to Snells law, when a photon encounters the interface of a medium of high refractive index n_1 with a medium of lower refractive index n_2. Part of the emission takes place within the escape cone, which is defined as the cone that is formed by the smallest angle of incidence for which total internal reflection occurs. This critical angle θ_c depends on the refractive indices of the two media $\theta_c = sin^{-1}(n_1/n_2)$. For the PMMA/air interface the critical angle is $\theta_c = 41.970°$. For the case of a luminophore that emits isotropically the probability that an emitted photon will remain inside the waveguide then is 0.7435.

Fig. 2a gives a visual representation of calculated efficiency losses using the ray-trace simulation model *pvtrace* [26] by presenting the photon destination in a simulated LSC matrix when it is exposed to sunlight. The LSC is doped with Lumogen F305 dye at a concentration of 184ppm with dimensions 5 cm × 5 cm × 0.3 cm, the LQE was set to 95%. As expected, photons at wavelengths outside of the absorption spectrum of the dye (Fig. 2b) are not absorbed and therefore are transmitted through the LSC plate.

2.4. Reabsorption

The loss mechanisms described above assume that there is a single photon absorption and emission event. However, the majority of the luminophores are characterized by an overlap between their absorption and emission spectra, which leads to reabsorption and reemission of the photon by (neighboring) luminophore(s). And while that might not directly lead to energy loss, the re-emitted light may experience all above-mentioned loss mechanisms several times in a row. The magnitude of this effect can also be seen in Fig. 2a, where according to the model, only 25.7% of all emitted photons are expected to escape either from the top of the bottom surface and 5%(1−LQE) would undergo non-radiative recombination. However, photons in the region 500–600 nm are subjected on average to 42% escape cone losses and 23.6% quantum yield losses.

Consequently, the larger the spectral overlap; the greater will be the energy loss of the LSC device. This can be quantified as reabsorption cross section σ_{SA} per centimeter of optical path taking into account absorption $A(\lambda)$ and emission $E(\lambda)$ spectra, as follows [17]:

$$\sigma_{SA} = \frac{\int A(\lambda)E(\lambda)d\lambda}{\int E(\lambda)} \tag{6}$$

A direct effect of reabsorption is the drop in luminescence intensity with increasing optical path length [27], which is undoubtedly the main reason for the dramatic drop in efficiency for large LSC devices. The decrease in intensity can partially be compensated by an increase in luminophore concentration as was proposed by Goetzberger and Greubel [12] and was later experimentally validated by Krumer [17] for Lumogen F305. This loss can be calculated using [17]:

$$\frac{\Phi_{LSC}}{\Phi_{in}} = \eta_{abs}(1 - \eta_{int})^{\langle N_{SA}\rangle} \tag{7}$$

which describes the relationship between the power flux of the edge emission Φ_{LSC} and the incident power flux on the top surface of the LSC Φ_{in}, as a function of the absorption efficiency of the luminophore η_{abs} the internal optical efficiency η_{int} and the average number of reabsorption events $\langle N_{SA}\rangle$. The value of the edge emission power flux, and consequently the device efficiency, depends on whether the absorption efficiency increases faster than $(1 - \eta_{int})^{\langle N_{SA}\rangle}$ upon the increase of dye concentration.

The most representative and quantitative indicator to describe reabsorption is the difference between absorption and emission spectrum, which is directly associated with the Stokes-shift. However, by comparing the absorption coefficient a_1 in the part of the spectrum where light absorption occurs, with the absorption coefficient a_2 at the state where photoluminescence takes place one can deduce a quality factor $Q = a_1/a_2$. A high value of the quality factor indicates that less reabsorption takes place and therefore higher device efficiency can be expected. Additionally, this quantity can directly be associated with the prospective performance of an LSC device, as it can be used to estimate the maximum optical concentration factor C_0 for given dimensions through the relationship $C_0 = FQ_{LSC}$ [18], with F being a numerical factor determined by the quantum efficiency and refractive index of the matrix [18].

3. Luminophores

Clearly, luminophores are the most critical part of an LSC, as they are the key elements that allow concentration through absorption and reemission of light. Primarily, luminescent species should be able to collect as many photons as possible and therefore they should exhibit a broad absorption spectrum combined with high absorption efficiency. A high LQE value close to 100% is also necessary to avoid quantum yield

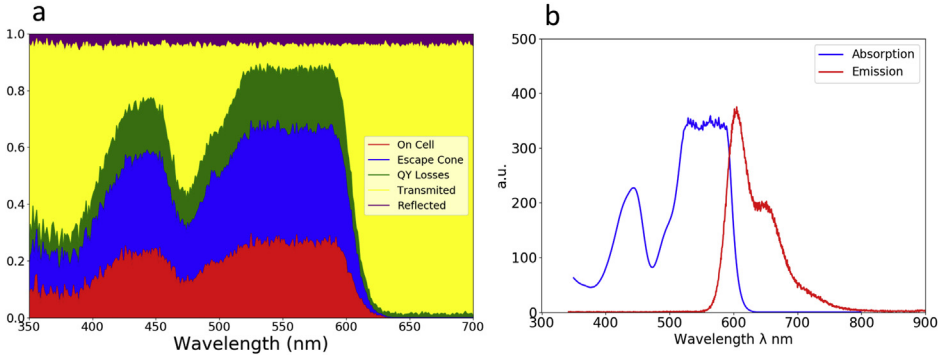

Fig. 2. a) Photon destination (color coded) for a simulated LSC device doped with Lumogen F305 dye, as a function of wavelength, b) Absorption and Emission Spectrum of Lumogen F305. (For interpretation of the references to color in this figure legend, the reader is referred to the Web version of this article.)

losses and a large Stokes-shift is needed to ensure minimum reabsorption. Since in most cases luminophores are incorporated in a polymeric host material, they should exhibit good solubility without negatively affecting the rest of their properties and demonstrate photostability appropriate for long term solar energy conversion applications, i.e. 30 year outdoor exposure.

3.1. Organic dyes

Organic dyes have been the first and probably the most researched luminophores for LSC applications mainly due to their high quantum yield and good solubility in polymer matrices [14]. The most commonly used types of dyes in the last decades have been the rhodamines, coumarins, and perylene derivatives. Rhodamine 6G was one of the first dyes explored because it exhibits high quantum yield [11], while the Lumogen series developed by BASF, which combine high quantum yield and low degradation rate for outdoor applications [10], were specifically designed for LSCs and for many years had the role of workhorse dye in LSC applications [28].

On the other hand, organic dyes are able to convert only a small fraction of the solar spectrum since they usually exhibit a narrow absorption band in the UV and visible part of the spectrum. To overcome that, a combination of different dyes that is able to absorb in different parts of the spectrum can be used, either as a stack of LSC plates or as a cocktail of dyes in a single LSC [14]. However, their emission spectrum is located in the visible range, which has significantly higher energy than the band gap of silicon, leading to spectral mismatch and thermalization losses. Also, the large spectral overlap, which is the cause of reabsorption losses is prohibiting the creation of large scale efficient devices. This is the reason for the absence of commercial applications of LSCs so far [29].

The reason behind the unsuccessful attempts to create efficient LSC devices using organic dyes lies within their chemical structure [7]. Planar π-conjugated molecules having all the atoms of the conjugate chain linked with σ-bonds, owe their photoluminescence to the promotion of a π electron from the ground state to an excited state [14]. And since photoluminescence occurs from the light absorbing state, the resulted Stokes-shift is relatively small. Additionally, the peak of the main absorption band is dictated primarily by the chain length [30] and therefore any efforts to alter spectral coverage would lead to instability of the dye structure and reduce photoluminescence (PL) yield.

3.2. Rare earth ions

An interesting alternative for luminophores in LSCs are luminescent rare earth ions such as lanthanide complexes (Ln^{3+}). Their unique optical properties such as large Stokes-shift, increased photostability, high quantum yield, broad absorption spectrum, and well defined narrow emission spectrum have attracted the attention of the scientific community from the very early days of LSC development [31]. Neodymium (Nd^{3+}) was introduced, together with Rhodamine 6G, in the original LSC research of Levitt and Weber already in 1977 [32]. However the doped glasses containing Neodymium performed poorly since the photons emitted at 880 nm were subjected to reabsorption and the reabsorption-free emission peak at 1060 nm is slightly below the band gap of silicon [33].

To increase the efficiency, the single ion approach where absorption takes place in the visible spectral range followed by relaxation to the lowest excited state was abandoned, and gave way to a combination of two ions. In this case one ion (the sensitizer) absorbs the light and subsequently transfers the energy to a second ion (the activator), which emits efficiently in the NIR. Such an example is the combination of Neodymium (Nd^{3+}) with Ytterbium (Yb^{3+}) where the energy absorbed from Neodymium is transferred to Ytterbium which emits at 970 nm [33]. The energy emitted at this wavelength offers a relatively high response, compared to the single-ion case above, despite being still only slightly higher than the band gap of silicon. However, even though the energy transfer efficiency can reach 90% in tellurite and germanite glasses, the whole process is limited by low absorption efficiencies [34].

An alternative approach to increase absorption is to introduce organic ligands as Ln^{3+} ions can be complexed with a wide variety of organic molecules, which harvest the incoming irradiation and transfer energy efficiently onto the metal ions. The result is a very high Stokes shift that exceeds 200 nm and an additional protection of metal ions from vibrational coupling [35]. Europium (Eu^{3+}) based complexes with *LQE* reaching 60% have been used for fabrication of planar LSCs which performed similarly compared to using CdSe and ZnS QDs under solar simulator conditions exhibiting an optical efficiency of 0.43% [35]. Even higher *LQE* values of 80% have been reported for Eu^{3+} β-diketonate complexes [36].

Another promising approach is to utilize LSC plates with Tm^{2+} in halides such as CaI2 or NaCl. The very broad absorption spectrum that goes up to 900 nm allows to absorb up to 63% of solar power while the emission at 1140 nm is an excellent match for a CIGS solar cell [37].

Finally, despite the promising features of lanthanide complexes the photodegradation due to UV exposure and the rather low thermal and photochemical stability are serious drawbacks regarding any technological applicability [14].

3.3. Colloidal semiconductors

The novel and extraordinary properties of colloidal semiconductor nanocrystals have also attracted a lot of attention as potential luminophores for LSCs. The nanocrystal consists of an inorganic core, which is a combination of two or more materials, coated by an organic layer of ligand surface molecules [38]. Different properties arise from different selection of materials, properties that are also defined by the size and shape of the nanocrystal and can be further modulated by the organic ligand surface layer [39].

The ability to control the size of the nanocrystal, which can vary between a few hundred to a few thousand atoms, is what allows one to fully exploit and engineer material properties. By decreasing the dimensions of the core, spatial quantum confinement effects become highly important and result in an increase in the band gap energy and the energy level separation between the electronic states [40]. Consequently, photoluminescence turns into a completely tunable property through a wide spectral window. Moreover, as the size of the nanocrystal decreases, the surface-to-volume ratio increases dramatically and as a result the nanocrystal becomes easily dispersible in solvents. Solubility is a clear advantage of colloidal chemistry for cheaper fabrication and processing of nanocrystals [38]. However, since the high population of surface atoms with fewer neighbors there is a significant amount of unsaturated bonds. These unshared orbitals create surface and trap states, which act as non-radiative recombination channels for the photoexcited charge carriers and thereby reduce the photoluminescence of the nanocrystal [41]. A well-established strategy to reduce these effects and improve surface passivation of the nanocrystal is to overgrow a shell of a wider band gap semiconductor, resulting in a core/shell system. Besides chemical stability, the coating offers the possibility to further tune absorption and emission in a larger spectral window than with both materials separately [38] (see Fig. 3a).

Specifically, by applying a shell of a wider band gap semiconductor, such as a ZnS or CdS shell around a CdSe core, a so-called Type I QD is created [38], see Fig. 3b. The shell acts as a light harvesting antenna especially for high energy photons, after which a very rapid energy relaxation to the core takes place. Since the shell has a larger band gap than the core, it confines both the electron and the hole in the core, which is now electronically isolated from the surrounding medium. As the exciton is no longer influenced by the dangling surface orbitals, the photoluminescence is increased and the stability against photodegradation is enhanced [42]. In a Type I core-shell particle, absorption and emission spectra depend on the core thickness and shell diameter.

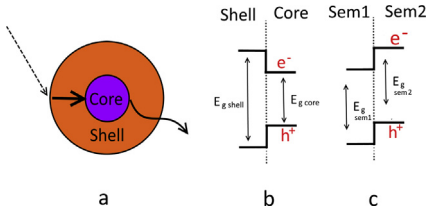

Fig. 3. a) Schematic representation of photon absorption, relaxation to the core and emission. b) Core and shell valence and conduction band energy level for Type I QDs. c) Semiconductor 1 and Semiconductor 2 conduction and valence band energy levels for Type II QDs.

As the shell becomes thicker, it dominates absorption and shields the core from lower energy photons, while it enhances photoluminescence [43]. Additionally, a redshift in the emission spectrum is also observed due to longer recombination times, increasing even further the Stokes-shift. In a "giant shell" QD, coated with 14 monolayers of CdS, optical efficiency was reported to reach 48%, with a *LQE* value at 86% for CdSe QDs, analogous to the most efficient low reabsorption organic systems [43]. However, for a similar QD configuration, it was observed that the thick shell was responsible for a 60% drop in photoluminescence for an optical path of 20 cm due to light scattering [44]. Light scattering might have a weaker effect over reabsorption [44], but combined with the limited spectral coverage inherent to the absorption profile of the shell, it results in strong limitations to the development of large scale LSC devices.

Instead of using a shell for confining both carriers in the same part of the nanocrystal, it is possible to spatially separate the hole and the electron by adjusting the band offset alignment between the core and the shell. As can be seen in Fig. 3c, the lowest energy states for a Type II QD are located in different parts of the particle and therefore we have the creation of an indirect exciton [42]. In this case the shell is not just a method for carrier confinement and passivation of the surface against the surrounding environment but also a tool to further tune emission wavelength to a range that otherwise would not be accessible. By controlling the core diameter and the shell thickness, and therefore the relative energy offset, the degree of charge carrier localization can be adjusted. The radiative recombination of the spatially indirect exciton that is created, will lead to emission energies lower than those of shell and core material independently, making Type II excellent candidates for near infrared emission [40]. Carrier delocalization is essential for absorption and emission control but at the same time the slower radiative recombination of the spatially indirect exciton triggers faster non-radiative processes that lead to poor *LQE* values in the range of $0-10\%$ for CdTe/CdSe and ZnTe/CdSe QDs [38]. However, what seemed to be an intrinsic weakness of Type II QDs was minimized by developing preparation technologies that could reduce surface and trapping defects of the nanocrystal leading to *LQE* values close to 80% [41].

Emission close to NIR is very significant for the development of LSCs mainly for two reasons. The first has to do with the energy distribution within the solar spectrum. By confining absorption to the ultraviolet and visible spectrum (usually below 500 nm for most of luminophores) about 60% of solar irradiation stays unabsorbed. Equally important is the right spectral match with the solar cell. LSCs are not energy converting devices, for that they rely on the solar cells, which are most commonly mounted on the edge(s) of an LSC plate. In particular the standard Si solar cell, which is used in most applications, operates in the spectral region between 400 and 1000 nm, perfectly matching the emission from NIR luminophores. By improving the external quantum efficiency of Si cells the entire power conversion efficiency of the device will be enhanced, even if all the other parameters remain unchanged [45]. Additionally, absorption that extends to the NIR and covers more or less uniformly also the entire visible spectrum makes it easier to fabricate colorless and semitransparent LSCs for windows applications.

Lead chalcogenides, such as PbSe and PbS were identified as interesting candidates since they both offer efficient and widely tunable emission in the infrared part of the spectrum [46]. Early attempts to fabricate LSCs using PbS QDs, that have spectral coverage up to 800 nm, exhibited an optical efficiency of 1.4% for a geometrical concentration factor of 11 in a liquid solution [47]. Compared to CdSe/ZnS QDs that exhibit a Stokes-shift of 23 nm, the uncoated PbS show a much expanded shift of 122 nm [47]. However, to achieve equivalent absorbance with the CdSe/ZnS QDs, the PbS solutions concentration needs to be more than 10 times higher, leading to strong reabsorption. Furthermore, proceeding to dispersion of the PbS solution in a waveguide which is formed after incorporation in a polymer sheet would lead to a significant drop in PL due to the thermal and chemical sensitivity of the QDs [48]. By developing a CdS shell around the PbS core chemical stability was enhanced, and the Stokes-shift was increased while the quantum yield stayed fairly high, reaching 67% at the optimal shell thickness [49]. Incorporated in a PMMA slab the optical efficiency reached 6.1% for a geometrical factor of 10 [50]. By introducing ultra-small PbS QDs of 2.2 nm in diameter covered with a thin layer (0.1 nm) of CdS, a Stokes-shift of 0.36 eV was achieved with a *LQE* of 70% [51]. The emitted photons were in the range of 700–1100 nm, which is considered optimal for coupling with a Si solar cell. With a geometrical factor of 50 the optical efficiency was 1.2%, which is among the highest reported for QDs with similar geometrical factors, as shown in Table 1.

So far, emission was achieved by the recombination of an exciton that was delocalized over the entire nanocrystal, which caused to a greater or lesser extent overlapping between absorption and emission spectra and therefore reabsorption. By incorporating a small amount of a luminescence activator within the QD, new optically forbidden transitions were facilitated from localized states within the band gap of the materials. These impurity-doped nanocrystals have the benefit that emission occurring from these states is significantly downshifted compared to the QD semiconductor absorption and consequently reabsorption can be effectively eliminated. An even more interesting feature of this transition is that it is one directional, allowing emission but blocking absorption as a spin forbidden process [58]. Furthermore, compared to giant shell QDs that also limit reabsorption, doped QDs have typically small dimensions, avoiding losses caused by scattering.

By introducing Mn^{2+} impurities into a ZnSe nanocrystal, which has a direct band gap of approximately 3.1 eV, a sensitized emission is achieved at 2.1 eV through an intragap transition [59]. Coating these nanocrystals with a ZnS shell and incorporating them into a polymer sheet results in a reabsorption-free nanocrystal. The size tunable absorption is in the range of 350–450 nm and the emission transition is centered at 582 nm, creating a large Stokes-shift of approximately 1 eV. Impressively, the *LQE* is preserved at 53%, equal to immersing them in a toluene solution, and 37% of photons that harvested from the top surface of the concentrator end up at the device edges with a geometrical concentration factor of 22 [59]. The fact that absorption is restricted to the UV range has the benefit that the LSC slabs are almost transparent for visible light. However, only 10% of the incoming irradiation can be

Table 1
Properties of LSCs with nanoparticles and other luminophores.

Luminophore	Type of Luminophore	*LQE* [%]	η_{opt} [%]	*G*
PbS/CdS [51]	QD	70	1.2	50
CdSe/CdS [44]	QD	86	0.6	43
$CdSe/Cd_xPbS_{1-x}$ [52]	QD	40	1.15	52.5
PbS/CdS [47]	QD	50	1.1	50
$CuInSe_xS_{2-x}/ZnS$ [53]	QD	40	3.2	40
Si [54]	Silicon QD	46	2.85	46
C [55]	Carbon QD	–	4.75	8
$EuCl_3$ $6H_2O$/tta [35]	Ln^{3+} QD	60	0.43	–
$CsPb(Br_xI_{x-3})_3$ [56]	Perovskite QDs	20	2	45
LR F305 [57]	Dye	90	8.1	16

captured, thus letting 90% pass through. Moreover, despite the impressive Stokes-shift the emitted photons are not an excellent fit to Si cells. In an attempt to achieve emission at larger wavelengths Mn^{2+} was replaced by Cu^{+} as a dopant since acceptor-donor recombination is red-shifted by 0.5 eV from the absorption edge. The addition of In instead of ZnS resulted in heavy metal free $CuInS_2$/ZnS QDs with absorption extended to the visible and NIR part of the spectrum. This QD configuration did eliminate reabsorption neither boost *LQE* but achieved an impressive 3.2% power conversion efficiency while exhibiting an almost crystal-clear transparency [53]. A slightly different composition that was developed also with $CuInS_2$ as the core nanocrystal, but with a shell of CdS instead of ZnS, placed the absorption peak outside the UV region, at 570 nm and enhanced *LQE* to 86% while the emission was expanded from 480 to 1000 nm [60]. Despite not being reabsorption free, the excellent spectral coupling with Si cells, the high *QY*, and the enhanced ability to harvest more solar light indicated that these nanocrystals hold promise for the future. Direct comparison between core/shell heterostructured nanocrystals with doped nanocrystals under the same experimental conditions revealed that reabsorption was the major problem for the former case, while in the latter it is eliminated considerably and at the same time a greater fraction of the solar spectrum is absorbed and visible transparency is retained [61].

Colloidal chemistry undoubtedly had a crucial contribution to the phenomenal advances in the quest for suitable emitters for LSC technology. Despite this impressive growth the field remains vastly unexplored and new concepts emerge continuously, even in cases were photoluminescence seemed impossible. Surprisingly, one of the most promising materials to achieve reabsorption-free QDs, lies within one of the most abundant materials on Earth. Silicon so far has been intensively used for photodetectors and photovoltaic cells, however it was considered to be unattractive for light emitting devices. As an indirect band gap semiconductor, in its bulk form it requires the assistance of phonons to achieve optical recombination of the excitons. However, upon quantum confinement, Si nanocrystals change their electronic and optical properties and become strongly luminescent [62]. The emission and absorption spectrum is highly tunable from the visible to NIR by controlling the size of the nanoparticle, as is the case with all the QDs that were used earlier as luminophores. Initially, *LQE* was below 5% [62] but through surface passivation it can exceed 50% [63]. Meinardi et al. [54] report Si quantum dots emitting at 830 nm with an effective Stokes-shift of approximately 400 meV, which is comparable with state of the art doped and giant core QDs. Incorporated in a plate with dimensions of 12 cm × 12 cm × 0.26 cm a transparency of 75% in the visible spectrum was achieved and despite the average *LQE* of 46%, the power conversion efficiency reached 2.85% [54]. This very promising result was accomplished with uncoated Si QDs, in contrast with CuInSeS and CdSe QDs which require an additional protective shell to preserve optical properties in a polymer slab.

Silicon QDs pose also the beneficial property to be composed of the most abundant material on Earths crust. The unmatched availability of these resources can be of a great importance for a future new born LSC industry for BIPV applications. Other solutions that would involve the use of indium or selenium could be hindered by the scarcity of raw materials and high prices. Practical and sustainable solutions also require non toxicity and environmental safety, which, beside Si, are also exhibited by the newly emerging carbon QDs. Discovered just in 2004 they are characterized by stability, ease of fabrication and low cost, while the first LSC application resulted in 3.94% power conversion efficiency [64].

Lead halide perovskites have also emerged as potential candidates for a variety of optoelectronic applications spanning from photovoltaic cells to lasers. The manganese doped perovskite nanocrystal shares the same tunable and size dependent absorption and emission spectrum as the rest of the QD family members but with two very distinctive emission peaks at 395 and 590 nm. The current *LQE* value does not exceed 10% though and the emission at the first peak is subjected to reabsorption [65]. Therefore the first attempt to create an LSC device resulted in a relatively poor 0.5% power conversion efficiency [65]. Since the development of perovskite QDs is still in an embryonal phase, advances in suppression of carrier trapping [66] and impurity doping [56] are expected to improve *LQE* and increase Stokes shift respectively.

The low *LQE* is one of the major issues that QDs face till now and so far, it blocks the road to energy efficiencies exceeding 10%. However, a newly emerged strategy attempts to elegantly circumvent that by combining two different luminophores through Förster resonance energy transfer (FRET). FRET is a mechanism of energy transfer between two light-sensitive molecules [67] that are very close to each other, which involves a donor particle which is in an excited state and transfers energy to an acceptor particle through non radiative dipole-dipole coupling. In this case a QD with the broad and tunable absorption spectrum is the donor but instead of emitting a photon itself, it is paired to an organic dye which has a higher *LQE* value. The long exciton lifetimes of QDs, usually 10 times larger than those of organic dyes, make it easier for FRET decay to take place [68]. This organic-inorganic cooperation requires cautious tuning: although a high concentration of organic dyes would improve the energy transfer, too much of it would increase reabsorption. Nevertheless, LSCs utilizing this combination showed an efficiency improvement of 24.7% relative to LSCs with QDs as the only luminophore [69].

An alternative approach to more effectively using the solar spectrum is actually inspired by conventional solar cell engineering. Like tandem PV, in which vertical integration of separate solar cells is realized, and in which each cells is specifically tailor-made for a specific part of the spectrum, tandem LSCs utilize multiple LSC elements with different spectral sensitivity. For example, the tandem LSC device that was created by Wu et al. [70] had a total surface area of 230 cm^2 and consisted of two LSC plates. The top layer was embedded with Mn^{2+} doped $Cd_xZn_{1-x}S$ QDs which have an absorption onset at 440 nm and due to the manganese ions the reabsorption is totally eliminated. The idea is to capture the high energy photons in the UV part of the spectrum as efficiently as possible while the escaped and unabsorbed light is utilized by the second layer. A bottom sheet incorporating narrower band gap $CuInSe_2$ QDs coated with a ZnS shell was chosen for that purpose. With a wider absorption spectrum and emission at 805 nm, it is able to absorb efficiently up to the NIR. However, the reabsorption effects did not allow the optical efficiency to surpass 24%. Despite the low absorptivity which is intrinsic of the Mn^{2+} doped QDs the total efficiency of the device reached 3.6% with visible transmittance of 23%. The cost efficiency of this device was at 0.87, which means that it can be 13% more cost efficient compared to conventional Si PV modules [70].

3.4. Degradation

While the focus is to create luminophores with high *LQE* and broad absorption spectrum, one of the major challenges that LSC technology still needs to overcome, is long term stability under outdoor conditions. Conventional PV exhibits exceptional stability with approximately only 20% decrease in performance in 20 years. Therefore commercialization will not be viable in the case of LSCs if operational lifetime is below 10 years [71]. However for both organic dyes and QDs, photodegradation represents the most common pathway towards performance decline.

For QDs, interaction with high energy photons launches photoreactions on the surface of the nanocrystals. The dissociation of molecular oxygen under the influence of the excited carriers in the QDs results in the oxidation of the semiconductors [72]. In the case of CdS, the nanocrystals are photo-oxidized to Cd^{2+} and SO_4^{2-} [73], and for the CdSe nanocrystals the result is the formation of SeO_2 and $CdSe_x$ (x = 2 and x = 3) [74,75]. Therefore upon photo-oxidation the effective QD core decreases in diameter resulting in a characteristic blue shift in the emission wavelength that varies up to 30–40 nm accompanied with a

gradual decrease in the photoluminescence intensity [76].

However, photoluminescence degradation and spectral blue shift is observed even with coated QDs. The occurrence of photooxidation in zinc coated QDs indicates that there is not a uniform crystalline overlayer of ZnS around a core but rather a layer with grain boundaries [76]. Therefore it is obvious that oxygen diffusion through the shell is still possible, which can be attributed to the lattice mismatch [77], as in the case of zinc blende CdTe and CdS (12%). By increasing the shell thickness, the oxidation rate is reduced due to slower diffusion of the oxygen to the core. However, the reduction of the core size alone cannot explain the complete bleaching of the QDs. It is more likely that non-radiative recombination pathways are created due to the formation of lattice defects in the QD that eventually result in the final bleaching [78].

3.5. Hosts and waveguides

One of the most significant elements of an LSC is the host material as it is fundamental for the operation and the electrical output of each device. Today the most common optical medium is poly (methyl methacrylate) (PMMA) followed by Poly-carbonate (PC) based formulations and glass [14]. Apart from high transparency in the visible and NIR part of the spectrum, which is essential to ensure an unobscured flux of photons, the waveguide should be able to satisfy a long list of features, essential for the optimum operation of an LSC.

The most representative tradeoff in the host material design process is the choice of the right refractive index. Minimization of the reflectance at the front surface is obviously desirable, as it allows for more light to enter the device. This requires a low refractive index. However, a low refractive index is not beneficial for maintaining a high total internal reflection rate as low values will lead to high critical angles and an widening of the escape cone. The optimum value for this process is set to be around $n = 2$ however the current compromise is a value closer to $n = 1.5$ as it is more common for most of the polymer and glass hosts [79]. The host material should also provide a high level of solubility of the luminophore to achieve maximum dissolution, while in the opposite case material aggregation can lead to non-uniform distribution of the luminophore in the matrix and the formation of scattering centers. Additionally it should provide a compatible processing temperature with the given luminophore and the ability to be optically coupled with PV cells. Taking into account the industrial process and the requirements of the BIPV industry the waveguide should comply with environmental and safety regulations, be light weight and stable under various weather conditions.

Glass is a material with excellent optical properties that can provide durability and compliance with fire regulations. It is environmentally stable and has already been part of the building industry for centuries. However, the extremely high temperatures required for the manufacturing of glass that can exceed 1100° C, are prohibiting the use of a majority of luminophores, which in case of the organic dyes can tolerate a temperature of only 300° C [80]. On the other hand polymer plates exhibit exceptional transparency in the visible and NIR part of the spectrum and high solubility for the majority of the luminophores that have been used so far. Comparison of different materials including glass, quartz plates, and different types of polymers revealed that reflection losses were in the range of 7–11% and that quartz has the best optical transparency followed by PMMA [81]. Since large quartz waveguides cannot be considered an economically viable option, focus was drawn once more to commercially available solutions. Measurements on optical density and optical efficiency of 8 different doped and undoped polymeric host matrices revealed that PMMA and PCCD (poly (1,4cyclohexylenedimethylene 1,4cyclohexanedicarboxylate)) outperformed all competitors [80]. However, the relatively small difference between optical efficiency values indicates that economic and secondary properties such as lifetime will play a major role in BIPV integration.

4. Applications

A number of losses, especially self-absorption and low *LQE* values, have hindered LSCs to achieve the efficiency values that would pave the way to commercialization. And while for the majority of solar harvesting applications high efficiency and long term stability would be sufficient to open the door of the scientific laboratory to the outside world, in the case of BIPV sector the situation is radically different. By aiming to become a fully functional element of the building envelope implies compliance to a series of strict safety and structural regulations while at the same time the wellbeing of occupants is secured. But it is not just the LSC and QD technology that has to achieve a certain degree of maturity in order to be accepted as a member of the current energy production system. The transformation of a buildings envelope into an energy production one requires new mechanisms for (building) energy management. Extending that to hundreds of buildings in the same urban area and that would bring disruption to grid operation as well.

Large scale implementation requires long term testing and adaptation; however, several developers have already taken advantage of the design freedom and fabrication versatility of LSCs to create niche applications in various fields. One of the sectors that first recognized the potential of LSCs is greenhouse horticulture. Commercial greenhouses are mainly made of glass and most of the times expand to many acres of agricultural land. The energy demand varies depending on the cultivation but they typically consume a considerable amount of electricity for heating, ventilation, lighting, refrigeration, and water pumping. The luminophore of choice in the test facility located in California, USA was Lumogen R305 red dye embedded in a matrix on top of a clear waveguide [82] (Fig. 4a). This configuration was chosen to mitigate the strong reabsorption losses that accompany organic dyes, as photons could be trapped by the top coating but when emitted to the bottom waveguide they can travel longer pathways before being reabsorbed. Since a high level of transparency is not a requirement in greenhouse applications the Si PV cells were mounted horizontally at the bottom of the waveguide instead of at the edges in contrast to the typical LSC layout. The Si cells were cut in thin strips of 2×12.5 cm and only 13.9% of the back surface was covered. The 22.3 m^3 demonstrator greenhouse that was built was projected to generate 1342 kWh of electricity per year or 57.4 kWh/m^2 and compared to the reference case it produced 37% higher energy yields [82]. Regarding crop production it was already shown that the overall effect is neutral to positive [83]. Therefore, as an overall conclusion, this type of application besides the clean energy production and the economic benefit for growers has the advantage of using already existing infrastructure without compromising plant productivity.

The same configuration with Lumogen dyes and face mounted Si cells on the back of an LSC device was also used for the Leaf Roof project [84] (Fig. 4c). The aim of this application is to create a roof tile design inspired by the natural shape of tree leaves. Roofs covered with

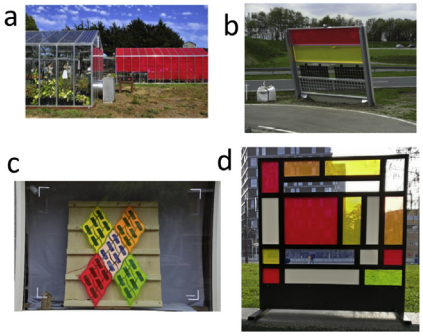

Fig. 4. a) LSC greenhouse in California, US [82]. b) Solar Noise Barrier project in 's Hertogenbosch, the Netherlands [85,86]. c) Leaf Roof [84]. d) The Electric Mondrian in Utrecht, the Netherlands [87].

LSC tiles, besides the aesthetic versatility, would also offer more freedom regarding the roof orientation and inclination as opposed to solar panel covered roofs. Because of the ability to harvest both direct and diffuse light, such roofs could potentially increase the generated electricity in Northern latitudes. At the same time this type of system would be less vulnerable to shading coming either from roof elements such as chimneys or from nearby buildings or trees. The Leaf Roof prototype has a surface area of 0.11 m^2 and 28.4% of this area is covered with PV cells. An energy yield of up to 9% higher is expected as compared to reference transparent waveguides [84].

The typical LSC layout with the edge mounted solar cells was used in some other applications. The first one was the solar noise barrier prototype along a highway outside of 's Hertogenbosch in the Netherlands [85,86] (Fig. 4b). The largest LSC plates constructed to date ($2 \times 5\ m^2$) were used in a test facility that measured performance under various environmental conditions for an application that could potentially be incorporated in many kilometers of noise barriers that are placed along highways, usually in close proximity to residential areas [85,86]. Finally, the Electric Mondrian is a case study of an LSC device that was created inspired by the painting style of Piet Mondrian. Colorful LSC plates embedded with Lumogen dyes were used to create a decorative element that could serve as a stand-alone charging point for mobile devices [87] (Fig. 4d). This is the first attempt to create an actual LSC as part of a window. The small size of the device, approximately 1 m^2, would not cause color distortion in the living space of the room behind it and the modularity of the system would allow larger or smaller areas to be covered.

5. Conclusion and discussion

In conclusion, as a result of the recent developments in the design of colloidal nanocrystals the combined targets of achieving LSCs with a broad spectral coverage and suppressed reabsorption has become feasible. Not only that, but with the introduction of greener production methods and the use of nontoxic, heavy metal free, and widely available materials as semiconducting materials it is clear that the scientific community has already taking steps to the next stage in QD development.

Despite the tremendous potential and the huge advancements in QD technology, the most heavily used luminophore so far, which still holds the efficiency record for a small device, is the organic dye. The question that is addressed in this paper, 18 years after the first QD LSC device was first described [29], is whether the QDs have become better luminophores than organic dyes. Comparative research has been conducted, already starting in 2007, between CdSe/ZnS and Lumogen F300 dye [14]. In that study, the QD reached 58% of the performance of the organic dye, mainly due to the low *LQE* of the nanocrystal molecules, which was in the range of 10 − 60% [64]. However, 10 years later, in 2017 Meinardi et al. set as a proper standard for comparison the equal spectral coverage of the luminophores [7]. This standard is crucial for the evaluation of reabsorption losses, as different concentrations are required for each chromophore to achieve a certain degree in spectral coverage. In a comparison using Monte Carlo based ray-trace simulations, the Lumogen Red LSC required a high dye concentration to achieve 30% spectral coverage while CuInSeS and PbS/CdS QDs with their broad absorption spectrum required a lower concentration and therefore reabsorption losses were drastically limited. Considering a hypothetical *LQE* value of 100% for all three luminophores the Lumogen dye LSC achieved 12.4% optical efficiency while the QD LSCs both surpassed 15% [7]. This illustrates the potential of QD LSCs to surpass the performance of dye LSCs.

The comparison between different types of QDs or QDs and organic dyes also within a wider perspective, the evaluation of transparent and semitransparent PV devices has raised the need of standardized methods of characterization and reporting. The BIPV sector and especially the facades and windows applications have to ensure a comfortable and healthy living environment. The human eye is very sensitive to long term exposure to color distortion in both domestic and working environments [88] and in some cases colored light can even have an effect on the human circadian rhythm [89]. While the power conversion efficiency is a widely used and acceptable key indicator for PV generators, it is unable to address any of the issues above. Therefore it was proposed by Traverse et al. [13] to use a weighted power conversion efficiency indicator with respect to the average visible transmission (AVT). The new indicator, light utilization efficiency (LUE), is the product of η_{device} and AVT and allows for a direct comparison between technologies for transparent and semitransparent applications [13].

There is still a great number of improvements that need to be accomplished regarding luminophore engineering before we consider LSCs as viable option for the urban environment. Nonetheless, the recent technological achievements have set LSCs on a clear path towards urban application. Undoubtedly, new challenges will emerge, and even if reabsorption is totally eliminated and *LQE* is close to 100%, it will still be a long way to waveguide optimization and solar cell coupling. However, LSCs are maybe the most unconventional type of solar energy technologies and the only technology with a huge potential to transform the future urban landscape.

Acknowledgement

This project is financially supported by Climate-KIC via the project Console, and by TKI-Urban Energy via the project Trapeze. We would like to thank Tim Prins (UU), Celso de Mello Donega (UU), Daniel Vanmaekelbergh (UU) and Dick de Boer (Philips Lighting) for fruitful discussions.

References

[1] A. Reinders, P. Verlinden, W. van Sark, A. Freundlich, Photovoltaic Solar Energy: from Fundamentals to Applications, John Wiley, Ltd, 2016, https://doi.org/10.1002/9781118927496.
[2] Energytrend, Global Solar Market to Reach over 106gw in 2018 Due to strong Momentum from China and Rebounding Demand in Europe, (Jan. 2018) https://pv.energytrend.com/research/Global_Solar_Market_to_Reach_Over_106GW_in_2018.html.
[3] C. Breyer, D. Bogdanov, A. Gulagi, A. Aghahosseini, L.S. Barbosa, O. Koskinen, M. Barasa, U. Caldera, S. Afanasyeva, M. Child, J. Farfan, P. Vainikka, On the role of solar photovoltaics in global energy transition scenarios, Prog. Photovoltaics Res. Appl. 25 (8) (2017) 727–745, https://doi.org/10.1002/pip.2885.
[4] A. Louwen, W.G.J.H.M. van Sark, A.P.C. Faaij, R.E.I. Schropp, Re-assessment of net energy production and greenhouse gas emissions avoidance after 40 years of photovoltaics development, Nat. Commun. 7 (2016) 13728, https://doi.org/10.1038/ncomms13728.
[5] W. Shockley, H.J. Queisser, Detailed balance limit of efficiency of p-n junction solar cells, J. Appl. Phys. 32 (3) (1961) 510–519, https://doi.org/10.1063/1.1736034.
[6] J.N. Mayer, Current and Future Cost of Photovoltaics. Long-term Scenarios for Market Development, System Prices and Lcoe of Utility-scale Pv Systems. Study on Behalf of Agora Energiewende, Tech. rep., Fraunhofer ISE, 2015.
[7] F. Meinardi, F. Bruni, S. Brovelli, Luminescent solar concentrators for building-integrated photovoltaics, Nature Reviews Materials 2 (12) (2017) 17072, https://doi.org/10.1038/natrevmats.2017.72.
[8] A.K. Shukla, K. Sudhakar, P. Baredar, Recent advancement in bipv product technologies: a review, Energy Build. 140 (2017) 188–195, https://doi.org/10.1016/j.enbuild.2017.02.015.
[9] M.G. Debije, Solar energy collectors with tunable transmission, Adv. Funct. Mater. 20 (9) (2010) 1498–1502, https://doi.org/10.1002/adfm.200902403.
[10] W.G. van Sark, K.W. Barnham, L.H. Slooff, A.J. Chatten, A. Büchtemann, A. Meyer, S.J. McCormack, R. Koole, D.J. Farrell, R. Bose, E.E. Bende, A.R. Burgers, T. Budel, J. Quilitz, M. Kennedy, T. Meyer, C.D.M. Donega, A. Meijerink, D. Vanmaekelbergh, Luminescent solar concentrators - a review of recent results, Optic Express 16 (26) (2008) 21773, https://doi.org/10.1364/oe.16.021773.
[11] W.H. Weber, J. Lambe, Luminescent greenhouse collector for solar radiation, Appl. Optic. 15 (10) (1976) 2299, https://doi.org/10.1364/ao.15.002299.
[12] W. G. A. Goetzberger, Solar energy conversion with fluorescent collectors, Appl. Phys.
[13] C.J. Traverse, R. Pandey, M.C. Barr, R.R. Lunt, Emergence of highly transparent photovoltaics for distributed applications, Nature Energy 2 (11) (2017) 849–860, https://doi.org/10.1038/s41560-017-0016-9.
[14] M.G. Debije, P.P.C. Verbunt, Thirty years of luminescent solar concentrator research: solar energy for the built environment, Advanced Energy Materials 2 (1)

(2011) 12–35, https://doi.org/10.1002/aenm.201100554.
[15] V. Wittwer, W. Stahl, A. Goetzberger, Fluorescent planar concentrators, Sol. Energy Mater. 11 (3) (1984) 187–197, https://doi.org/10.1016/0165-1633(84)90070-4.
[16] V. Wittwer, K. Heidler, A. Zastrow, A. Goetzberger, Theory of fluorescent planar concentrators and experimental results, J. Lumin. 24–25 (1981) 873–876, https://doi.org/10.1016/0022-2313(81)90108-3.
[17] Z. Krumer, W.G. van Sark, R.E. Schropp, C. de Mello Donega, Compensation of self-absorption losses in luminescent solar concentrators by increasing luminophore concentration, Sol. Energy Mater. Sol. Cell. 167 (2017) 133–139, https://doi.org/10.1016/j.solmat.2017.04.010.
[18] V.I. Klimov, T.A. Baker, J. Lim, K.A. Velizhanin, H. McDaniel, Quality factor of luminescent solar concentrators and practical concentration limits attainable with semiconductor quantum dots, ACS Photonics 3 (6) (2016) 1138–1148, https://doi.org/10.1021/acsphotonics.6b00307.
[19] L.H. Slooff, E.E. Bende, A.R. Burgers, T. Budel, M. Pravettoni, R.P. Kenny, E.D. Dunlop, A. Büchtemann, A luminescent solar concentrator with 7.1% power conversion efficiency, Physica Status Solidi (RRL) - Rapid Research Letters 2 (6) (2008) 257–259, https://doi.org/10.1002/pssr.200802186.
[20] J.C. Goldschmidt, M. Peters, A. Bösch, H. Helmers, F. Dimroth, S.W. Glunz, G. Willeke, Increasing the efficiency of fluorescent concentrator systems, Sol. Energy Mater. Sol. Cell. 93 (2) (2009) 176–182, https://doi.org/10.1016/j.solmat.2008.09.048.
[21] L. Desmet, A.J.M. Ras, D.K.G. de Boer, M.G. Debije, Monocrystalline silicon photovoltaic luminescent solar concentrator with 42% power conversion efficiency, Optic Lett. 37 (15) (2012) 3087, https://doi.org/10.1364/ol.37.003087.
[22] P. Friedman, Progress on the development of luminescent solar concentrators, Proc. Soc. Photo Opt. Instrum. Eng. 248.
[23] M.J. Currie, J.K. Mapel, T.D. Heidel, S. Goffri, M.A. Baldo, High-efficiency organic solar concentrators for photovoltaics, Science 321 (5886) (2008) 226–228, https://doi.org/10.1126/science.1158342.
[24] J. Roncali, F. Garnier, Photon-transport properties of luminescent solar concentrators: analysis and optimization, Appl. Optic. 23 (16) (1984) 2809, https://doi.org/10.1364/ao.23.002809.
[25] P. Bouger, Essai d' optique sur la gradation de la lumiere.
[26] Daniel, Achatten, Pvtrace, Release to Enable Doi Integration, (2014), https://doi.org/10.5281/zenodo.12820.
[27] R.W. Olson, R.F. Loring, M.D. Fayer, Luminescent solar concentrators and the reabsorption problem, Appl. Optic. 20 (17) (1981) 2934, https://doi.org/10.1364/ao.20.002934.
[28] G. Seybold, New perylene and violanthrone dyestuffs for fluorescent collectors, Dyes Pigments 11 (4) (1989) 303–317, https://doi.org/10.1016/0143-7208(89)85048-x.
[29] M. Debije, Semiconductor solution, Nat. Photon. 11 (3) (2017) 143–144, https://doi.org/10.1038/nphoton.2017.20.
[30] M. El-Shahawy, A. Mansour, Optical properties of some luminescent solar concentrators, J. Mater. Sci. Mater. Electron. 7 (3). https://doi.org/10.1007/bf00133110.
[31] M.M. Nolasco, P.M. Vaz, V.T. Freitas, P.P. Lima, P.S. André, R.A.S. Ferreira, P.D. Vaz, P. Ribeiro-Claro, L.D. Carlos, Engineering highly efficient eu(iii)-based triureasil hybrids toward luminescent solar concentrators, J. Mater. Chem. 1 (25) (2013) 7339, https://doi.org/10.1039/c3ta11463e.
[32] J.A. Levitt, W.H. Weber, Materials for luminescent greenhouse solar collectors, Appl. Optic. 16 (10) (1977) 2684, https://doi.org/10.1364/ao.16.002684.
[33] R. Reisfeld, Y. Kalisky, Nd3 and yb3 germanate and tellurite glasses for fluorescent solar energy collectors, Chem. Phys. Lett. 80 (1) (1981) 178–183, https://doi.org/10.1016/0009-2614(81)80084-x.
[34] C. Parent, C. Lurin, G.L. Flem, P. Hagenmuller, Nd^{+3} to yb^{+3}energy transfer in glasses with composition close to LiLnP4o12 metaphosphate (ln = la, nd, yb), J. Lumin. 36 (1) (1986) 49–55, https://doi.org/10.1016/0022-2313(86)90030-x.
[35] V.T. Freitas, L. Fu, A.M. Cojocariu, X. Cattoën, J.R. Bartlett, R.L. Parc, J.-L. Bantignies, M.W.C. Man, P.S. André, R.A.S. Ferreira, L.D. Carlos, Eu^{3+}-based bridged silsesquioxanes for transparent luminescent solar concentrators, ACS Appl. Mater. Interfaces 7 (16) (2015) 8770–8778, https://doi.org/10.1021/acsami.5b01281.
[36] S.F.H. Correia, V. de Zea Bermudez, S.J.L. Ribeiro, P.S. Andre, R.A.S. Ferreira, L.D. Carlos, Luminescent solar concentrators: challenges for lanthanide-based organic–inorganic hybrid materials, J. Mater. Chem. 2 (16) (2014) 5580–5596, https://doi.org/10.1039/c3ta14964a.
[37] O.M. ten Kate, K.W. Krämer, E. van der Kolk, Efficient luminescent solar concentrators based on self-absorption free, tm 2 doped halides, Sol. Energy Mater. Sol. Cell. 140 (2015) 115–120, https://doi.org/10.1016/j.solmat.2015.04.002.
[38] C. de Mello Donega, Synthesis and properties of colloidal heteronanocrystals, Chem. Soc. Rev. 40 (3) (2011) 1512–1546, https://doi.org/10.1039/c0cs00055h.
[39] S.A. Ivanov, A. Piryatinski, J. Nanda, S. Tretiak, K.R. Zavadil, W.O. Wallace, D. Werder, V.I. Klimov, Type-II core/shell CdS/ZnSe nanocrystals: synthesis, electronic structures, and spectroscopic properties, J. Am. Chem. Soc. 129 (38) (2007) 11708–11719, https://doi.org/10.1021/ja068351m.
[40] P. Reiss, M. Protière, L. Li, Core/shell semiconductor nanocrystals, Small 5 (2) (2009) 154–168, https://doi.org/10.1002/smll.200800841.
[41] P.T.K. Chin, C. de Mello Donega, S.S. van Bavel, S.C.J. Meskers, N.A.J.M. Sommerdijk, R.A.J. Janssen, Highly luminescent CdTe/CdSe colloidal heteronanocrystals with temperature-dependent emission color, J. Am. Chem. Soc. 129 (48) (2007) 14880–14886, https://doi.org/10.1021/ja0738071.
[42] C. de Mello Donega, Formation of nanoscale spatially indirect excitons: evolution of the type-II optical character of CdTe/CdSe heteronanocrystals, Phys. Rev. B 81 (16). https://doi.org/10.1103/physrevb.81.165303.
[43] I. Coropceanu, M.G. Bawendi, Core/shell quantum dot based luminescent solar concentrators with reduced reabsorption and enhanced efficiency, Nano Lett. 14 (7) (2014) 4097–4101, https://doi.org/10.1021/nl501627e.
[44] F. Meinardi, A. Colombo, K.A. Velizhanin, R. Simonutti, M. Lorenzon, L. Beverina, R. Viswanatha, V.I. Klimov, S. Brovelli, Large-area luminescent solar concentrators based on 'Stokes-shift-engineered' nanocrystals in a mass-polymerized PMMA matrix, Nat. Photon. 8 (5) (2014) 392–399, https://doi.org/10.1038/nphoton.2014.54.
[45] K.R. McIntosh, G. Lau, J.N. Cotsell, K. Hanton, D.L. Bätzner, F. Bettiol, B.S. Richards, Increase in external quantum efficiency of encapsulated silicon solar cells from a luminescent down-shifting layer, Prog. Photovoltaics Res. Appl. 17 (3) (2009) 191–197, https://doi.org/10.1002/pip.867.
[46] J.M. Pietryga, R.D. Schaller, D. Werder, M.H. Stewart, V.I. Klimov, J.A. Hollingsworth, Pushing the band gap envelope: mid-infrared emitting colloidal PbSe quantum dots, J. Am. Chem. Soc. 126 (38) (2004) 11752–11753, https://doi.org/10.1021/ja047659f.
[47] G.V. Shcherbatyuk, R.H. Inman, C. Wang, R. Winston, S. Ghosh, Viability of using near infrared PbS quantum dots as active materials in luminescent solar concentrators, Appl. Phys. Lett. 96 (19) (2010) 191901, https://doi.org/10.1063/1.3422485.
[48] W. Lü, I. Kamiya, M. Ichida, H. Ando, Temperature dependence of electronic energy transfer in PbS quantum dot films, Appl. Phys. Lett. 95 (8) (2009) 083102, https://doi.org/10.1063/1.3213349.
[49] H. Zhao, M. Chaker, N. Wu, D. Ma, Towards controlled synthesis and better understanding of highly luminescent PbS/CdS core/shell quantum dots, J. Mater. Chem. 21 (24) (2011) 8898, https://doi.org/10.1039/c1jm11205h.
[50] Y. Zhou, D. Benetti, Z. Fan, H. Zhao, D. Ma, A.O. Govorov, A. Vomiero, F. Rosei, Near infrared, highly efficient luminescent solar concentrators, Advanced Energy Materials 6 (11) (2016) 1501913, https://doi.org/10.1002/aenm.201501913.
[51] L. Tan, Y. Zhou, F. Ren, D. Benetti, F. Yang, H. Zhao, F. Rosei, M. Chaker, D. Ma, Ultrasmall PbS quantum dots: a facile and greener synthetic route and their high performance in luminescent solar concentrators, J. Mater. Chem. 5 (21) (2017) 10250–10260, https://doi.org/10.1039/c7ta01372h.
[52] H. Zhao, D. Benetti, L. Jin, Y. Zhou, F. Rosei, A. Vomiero, Absorption enhancement in "giant" core/alloyed-shell quantum dots for luminescent solar concentrator, Small 12 (38) (2016) 5354–5365, https://doi.org/10.1002/smll.201600945.
[53] F. Meinardi, H. McDaniel, F. Carulli, A. Colombo, K.A. Velizhanin, N.S. Makarov, R. Simonutti, V.I. Klimov, S. Brovelli, Highly efficient large-area colourless luminescent solar concentrators using heavy-metal-free colloidal quantum dots, Nat. Nanotechnol. 10 (10) (2015) 878–885, https://doi.org/10.1038/nnano.2015.178.
[54] F. Meinardi, S. Ehrenberg, L. Dhamo, F. Carulli, M. Mauri, F. Bruni, R. Simonutti, U. Kortshagen, S. Brovelli, Highly efficient luminescent solar concentrators based on earth-abundant indirect-bandgap silicon quantum dots, Nat. Photon. 11 (3) (2017) 177–185, https://doi.org/10.1038/nphoton.2017.5.
[55] Y. Li, P. Miao, W. Zhou, X. Gong, X. Zhao, N-doped carbon-dots for luminescent solar concentrators, J. Mater. Chem. 5 (40) (2017) 21452–21459, https://doi.org/10.1039/c7ta05220k.
[56] H. Zhao, Y. Zhou, D. Benetti, D. Ma, F. Rosei, Perovskite quantum dots integrated in large-area luminescent solar concentrators, Nanomater. Energy 37 (2017) 214–223, https://doi.org/10.1016/j.nanoen.2017.05.030.
[57] M. Carlotti, G. Ruggeri, F. Bellina, A. Pucci, Enhancing optical efficiency of thin-film luminescent solar concentrators by combining energy transfer and stacked design, J. Lumin. 171 (2016) 215–220, https://doi.org/10.1016/j.jlumin.2015.11.010.
[58] R. Beaulac, P.I. Archer, D.R. Gamelin, Luminescence in colloidal mn-doped semiconductor nanocrystals, J. Solid State Chem. 181 (7) (2008) 1582–1589, https://doi.org/10.1016/j.jssc.2008.05.001.
[59] C.S. Erickson, L.R. Bradshaw, S. McDowall, J.D. Gilbertson, D.R. Gamelin, D.L. Patrick, Zero-reabsorption doped-nanocrystal luminescent solar concentrators, ACS Nano 8 (4) (2014) 3461–3467, https://doi.org/10.1021/nn406360w.
[60] K.E. Knowles, T.B. Kilburn, D.G. Alzate, S. McDowall, D.R. Gamelin, Bright CuInS2/CdS nanocrystal phosphors for high-gain full-spectrum luminescent solar concentrators, Chem. Commun. 51 (44) (2015) 9129–9132, https://doi.org/10.1039/c5cc02007g.
[61] L.R. Bradshaw, K.E. Knowles, S. McDowall, D.R. Gamelin, Nanocrystals for luminescent solar concentrators, Nano Lett. 15 (2) (2015) 1315–1323, https://doi.org/10.1021/nl504510t.
[62] C. Meier, A. Gondorf, S. Lüttjohann, A. Lorke, H. Wiggers, Silicon nanoparticles: absorption, emission, and the nature of the electronic bandgap, J. Appl. Phys. 101 (10) (2007) 103112, https://doi.org/10.1063/1.2720095.
[63] R. Anthony, U. Kortshagen, Photoluminescence quantum yields of amorphous and crystalline silicon nanoparticles, Phys. Rev. B 80 (11). https://doi.org/10.1103/physrevb.80.115407.
[64] S. Gallagher, B. Norton, P. Eames, Quantum dot solar concentrators: electrical conversion efficiencies and comparative concentrating factors of fabricated devices, Sol. Energy 81 (6) (2007) 813–821, https://doi.org/10.1016/j.solener.2006.09.011.
[65] F. Meinardi, Q.A. Akkerman, F. Bruni, S. Park, M. Mauri, Z. Dang, L. Manna, S. Brovelli, Doped halide perovskite nanocrystals for reabsorption-free luminescent solar concentrators, ACS Energy Letters 2 (10) (2017) 2368–2377, https://doi.org/10.1021/acsenergylett.7b00701.
[66] B.A. Koscher, J.K. Swabeck, N.D. Bronstein, A.P. Alivisatos, Essentially trap-free CsPbBr3 colloidal nanocrystals by postsynthetic thiocyanate surface treatment, J. Am. Chem. Soc. 139 (19) (2017) 6566–6569, https://doi.org/10.1021/jacs.7b02817.
[67] J.R. Lakowicz (Ed.), Principles of Fluorescence Spectroscopy, Springer US, 2006, , https://doi.org/10.1007/978-0-387-46312-4.

[68] F. Grosse, E.A. Muljarov, R. Zimmermann, Phonons in quantum dots and their role in exciton dephasing, Semiconductor Nanostructures, Springer Berlin Heidelberg, 2008, pp. 165–187, , https://doi.org/10.1007/978-3-540-77899-8_8.
[69] C. Tummeltshammer, M. Portnoi, S.A. Mitchell, A.-T. Lee, A.J. Kenyon, A.B. Tabor, I. Papakonstantinou, On the ability of förster resonance energy transfer to enhance luminescent solar concentrator efficiency, Nanomater. Energy 32 (2017) 263–270, https://doi.org/10.1016/j.nanoen.2016.11.058.
[70] K. Wu, H. Li, V.I. Klimov, Tandem luminescent solar concentrators based on engineered quantum dots, Nat. Photon. 12 (2) (2018) 105–110, https://doi.org/10.1038/s41566-017-0070-7.
[71] B. Rowan, L. Wilson, B. Richards, Advanced material concepts for luminescent solar concentrators, IEEE J. Sel. Top. Quant. Electron. 14 (5) (2008) 1312–1322, https://doi.org/10.1109/jstqe.2008.920282.
[72] S. Sato, S. Nozaki, H. Morisaki, Photo-oxidation of germanium nanostructures deposited by the cluster-beam evaporation technique, J. Appl. Phys. 81 (3) (1997) 1518–1521, https://doi.org/10.1063/1.363917.
[73] S.F. Lee, M.A. Osborne, Brightening, blinking, bluing and bleaching in the life of a quantum dot: friend or foe? ChemPhysChem 10 (13) (2009) 2174–2191, https://doi.org/10.1002/cphc.200900200.
[74] J.E.B. Katari, V.L. Colvin, A.P. Alivisatos, X-ray photoelectron spectroscopy of CdSe nanocrystals with applications to studies of the nanocrystal surface, J. Phys. Chem. 98 (15) (1994) 4109–4117, https://doi.org/10.1021/j100066a034.
[75] A. Henglein, Mechanism of reactions on colloidal microelectrodes and size quantization effects, in: Topics in Current Chemistry, Springer-Verlag, pp. 113–180. https://doi.org/10.1007/bfb0018073.
[76] W.G.J.H.M. van Sark, P.L.T.M. Frederix, A.A. Bol, H.C. Gerritsen, A. Meijerink, Blueing, bleaching, and blinking of single CdSe/ZnS quantum dots, ChemPhysChem 3 (10) (2002) 871–879, https://doi.org/10.1002/1439-7641(20021018)3:10<871::aid-cphc871>3.0.co;2-t.
[77] N. Doskaliuk, Y. Khalavka, P. Fochuk, Influence of the shell thickness and ratio between core elements on photostability of the CdTe/CdS core/shell quantum dots embedded in a polymer matrix, Nanoscale Res. Lett. 11 (1). https://doi.org/10.1186/s11671-016-1428-3.
[78] S.A. Blanton, M.A. Hines, P. Guyot-Sionnest, Photoluminescence wandering in single CdSe nanocrystals, Appl. Phys. Lett. 69 (25) (1996) 3905–3907, https://doi.org/10.1063/1.117565.
[79] H. Ma, A.-Y. Jen, L. Dalton, Polymer-based optical waveguides: materials, processing, and devices, Adv. Mater. 14 (19) (2002) 1339–1365, https://doi.org/10.1002/1521-4095(20021002)14:19<1339::aid-adma1339>3.0.co;2-o.
[80] M. Zettl, O. Mayer, E. Klampaftis, B.S. Richards, Investigation of host polymers for luminescent solar concentrators, Energy Technol. 5 (7) (2017) 1037–1044, https://doi.org/10.1002/ente.201600498.
[81] M.J. Kastelijn, C.W. Bastiaansen, M.G. Debije, Influence of waveguide material on light emission in luminescent solar concentrators, Opt. Mater. 31 (11) (2009) 1720–1722, https://doi.org/10.1016/j.optmat.2009.05.003.
[82] C. Corrado, S.W. Leow, M. Osborn, I. Carbone, K. Hellier, M. Short, G. Alers, S.A. Carter, Power generation study of luminescent solar concentrator greenhouse, J. Renew. Sustain. Energy 8 (4) (2016) 043502, https://doi.org/10.1063/1.4958735.
[83] A.M. Detweiler, C.E. Mioni, K.L. Hellier, J.J. Allen, S.A. Carter, B.M. Bebout, E.E. Fleming, C. Corrado, L.E. Prufert-Bebout, Evaluation of wavelength selective photovoltaic panels on microalgae growth and photosynthetic efficiency, Algal Res. 9 (2015) 170–177, https://doi.org/10.1016/j.algal.2015.03.003.
[84] A.H.M.E. Reinders, G.D. de la Gree, A. Papadopoulos, A. Rosemann, M.G. Debije, M. Cox, Z. Krumer, Leaf roof — designing luminescent solar concentrating PV roof tiles, 2016 IEEE 43rd Photovoltaic Specialists Conference (PVSC), IEEE, 2016, , https://doi.org/10.1109/pvsc.2016.7750307.
[85] M. Kanellis, M.M. de Jong, L. Slooff, M.G. Debije, The solar noise barrier project: 1. effect of incident light orientation on the performance of a large-scale luminescent solar concentrator noise barrier, Renew. Energy 103 (2017) 647–652, https://doi.org/10.1016/j.renene.2016.10.078.
[86] M.G. Debije, C. Tzikas, V.A. Rajkumar, M.M. de Jong, The solar noise barrier project: 2. the effect of street art on performance of a large scale luminescent solar concentrator prototype, Renew. Energy 113 (2017) 1288–1292, https://doi.org/10.1016/j.renene.2017.07.025.
[87] W. van Sark, P. Moraitis, C. Aalberts, M. Drent, T. Grasso, Y.L. Ortije, M. Visschers, M. Westra, R. Plas, W. Planje, The “electric mondrian” as a luminescent solar concentrator demonstrator case study, Solar RRL 1 (3–4) (2017) 1600015, https://doi.org/10.1002/solr.201600015.
[88] F.M. Vossen, M.P. Aarts, M.G. Debije, Visual performance of red luminescent solar concentrating windows in an office environment, Energy Build. 113 (2016) 123–132, https://doi.org/10.1016/j.enbuild.2015.12.022.
[89] D.M. Berson, Phototransduction by retinal ganglion cells that set the circadian clock, Science 295 (5557) (2002) 1070–1073, https://doi.org/10.1126/science.1067262.